



HAL
open science

Isotropic dry etching of Si selectively to Si_{0.7}Ge_{0.3} for CMOS sub-10 nm applications

Sana Rachidi, Alain Campo, Virginie Loup, Christian Vizioz, Jean-Michel Hartmann, Sébastien Barnola, Nicolas Posseme

► **To cite this version:**

Sana Rachidi, Alain Campo, Virginie Loup, Christian Vizioz, Jean-Michel Hartmann, et al.. Isotropic dry etching of Si selectively to Si_{0.7}Ge_{0.3} for CMOS sub-10 nm applications. *Journal of Vacuum Science & Technology A*, 2020, 38 (3), 10.1116/1.5143118 . cea-04947561

HAL Id: cea-04947561

<https://cea.hal.science/cea-04947561v1>

Submitted on 14 Feb 2025

HAL is a multi-disciplinary open access archive for the deposit and dissemination of scientific research documents, whether they are published or not. The documents may come from teaching and research institutions in France or abroad, or from public or private research centers.

L'archive ouverte pluridisciplinaire **HAL**, est destinée au dépôt et à la diffusion de documents scientifiques de niveau recherche, publiés ou non, émanant des établissements d'enseignement et de recherche français ou étrangers, des laboratoires publics ou privés.



RESEARCH ARTICLE | MARCH 09 2020

Isotropic dry etching of Si selectively to $\text{Si}_{0.7}\text{Ge}_{0.3}$ for CMOS sub-10 nm applications

Sana Rachidi; Alain Campo; Virginie Loup; Christian Vizios; Jean-Michel Hartmann; Sébastien Barnola; Nicolas Posseme



J. Vac. Sci. Technol. A 38, 033002 (2020)

<https://doi.org/10.1116/1.5143118>



View
Online



Export
Citation



Advance your science and
career as a member of

AVS

LEARN MORE



Isotropic dry etching of Si selectively to Si_{0.7}Ge_{0.3} for CMOS sub-10 nm applications

Cite as: J. Vac. Sci. Technol. A 38, 033002 (2020); doi: 10.1116/1.5143118

Submitted: 19 December 2019 · Accepted: 21 February 2020 ·

Published Online: 9 March 2020



Sana Rachidi,^{a)} Alain Campo,^{b)} Virginie Loup,^{c)} Christian Vizioz,^{d)} Jean-Michel Hartmann,^{e)} Sébastien Barnola,^{f)} and Nicolas Posseme^{g)}

AFFILIATIONS

Université Grenoble Alpes and CEA, LETI, Grenoble 38000, France

^{a)}Electronic mail: sana.rach92@gmail.com

^{b)}Electronic mail: alain.campo@cea.fr

^{c)}Electronic mail: virginie.loup@cea.fr

^{d)}Electronic mail: christian.vizioz@cea.fr

^{e)}Electronic mail: jean-michel.hartmann@cea.fr

^{f)}Electronic mail: sebastien.barnola@cea.fr

^{g)}Electronic mail: nicolas.posseme@cea.fr

ABSTRACT

The fabrication of Si_{0.7}Ge_{0.3} sub-10 nm nanochannels in gate-all-around devices requires a highly selective Si isotropic etching process. The etching of Si selectively to Si_{0.7}Ge_{0.3} with CF₄/N₂/O₂ downstream plasma has been investigated using various morphological and surface characterization techniques. Conditions such as 400 W microwave power, 700 mTorr pressure, 25 °C chuck temperature, and 22% CF₄:22% N₂:56% O₂ feed gas mixture were found to be optimum for selectivity and etch rates. X-ray photoelectron spectroscopy showed that, during the etching process, a highly reactive 8 nm thick SiO_xF_y layer is formed on Si. Meanwhile, a 2 nm thick passivation layer is observed on SiGe. The latter is a mixture of SiO_xF_y and GeO_xF_y species that protected the alloy from etching. The process selectivity was improved by investigating different wet and dry oxidant treatments prior to etching. The dry oxidant treatment gives the best results in terms of selectivity. These results obtained on blanket wafers have been validated on pattern wafers. Scanning electron microscopy demonstrated that SiGe nanowires were fully released with a high selectivity after dry oxidation followed by the etching process.

Published under license by AVS. <https://doi.org/10.1116/1.5143118>

I. INTRODUCTION

Maintaining a high drive current with low off-current leakage and controlling short channel effects are the main challenges that limit further downsizing of complementary metal oxide semiconductor (CMOS) devices. Gate-all-around (GAA) architectures are ideal to have sub-10 nm CMOS transistors with high current drivability, thanks to vertically stacked channels while overcoming the above-mentioned challenges.^{1,2} Stacked nanowire (SNW) devices are fabricated thanks to the epitaxial growth of SiGe/Si multilayers, selective etching, and conformal deposition of dielectrics/metal gate stacks in-between the nanowires. A highly selective isotropic etching between the sacrificial layers and the channel layers of interest is then mandatory. Several studies^{3,4} have been published on the use of SiGe as sacrificial

layers to be etched selectively versus Silicon in order to fabricate Si GAA-CMOS devices. Compressively strained SiGe layers could, however, be used as pMOS GAA channels. The hole mobility in compressively strained SiGe is indeed two to three times that in pure, unstrained Silicon.^{5,6}

These compressively strained SiGe layers are then surrounded by Si layers, which have to be selectively removed to obtain high hole-mobility SiGe stacked channels in the end. During isotropic etching, Si and SiGe layers are exposed to the reactive etchants. A very high selectivity is then needed to have ultimately the SiGe layers aimed for, with ideally, no shape change (i.e., little or no thinning, no widening at the entrance of tunnels, and so on).

In this article, we investigated the isotropic etching of Si selectively to Si_{0.7}Ge_{0.3} using downstream CF₄/O₂/N₂ plasma chemistry.

14 February 2025 09:46:34

From x-ray photoelectron spectroscopy (XPS) and time-of-flight-secondary ion mass spectrometry (ToF-SIMS), an etching mechanism for Si and SiGe will be proposed. Process optimization through the use of dry oxidation prior to etching will also be presented. Finally, we will show that the $\text{CF}_4/\text{N}_2/\text{O}_2$ process can be used on small dimensions patterned structures to fabricate stacked SiGe NWs.

II. EXPERIMENT

A. Materials description

In this study, two sets of samples have been used: (1) fullsheet Si and SiGe layers deposited on silicon-on-insulator (SOI) substrates for characterization and optimization of the etching process and (2) patterned wafers of two period (Si \sim 8 nm/ $\text{Si}_{0.7}\text{Ge}_{0.3}$ \sim 8 nm) superlattices on SOI substrates. Blanket layers or superlattices were epitaxially grown by reduced pressure-chemical vapor deposition in an ASM Epsilon 3200 tool or in the RP (reduced pressure) chamber, a 300 mm Centura cluster tool from Applied Materials. Growth temperatures and pressures were 650 °C and 20 Torr in both chambers. SiH_4 was used as the gaseous precursor during the epitaxy of Si (with a growth rate around 10 nm/min), while SiH_2Cl_2 and GeH_4 were the precursors adopted for the growth of $\text{Si}_{0.7}\text{Ge}_{0.3}$ (with a growth rate around 25 nm/min). The ultrapure H_2 carrier flow, a few tens of standard liters/minute, was the same throughout the study. The $\text{F}(\text{SiH}_4)/\text{F}(\text{H}_2)$ mass-flow ratio was equal to 0.012, while the $\text{F}(\text{SiH}_2\text{Cl}_2)/\text{F}(\text{H}_2)$ and $\text{F}(\text{GeH}_4)/\text{F}(\text{H}_2)$ mass-flow ratios were equal to 0.003 and 0.00025, respectively.

Patterns have been fabricated as follows: a 2.5 nm thick SiO_2 layer is deposited on the superlattices, with on top, a bottom anti-reflectant coating and a photoresist. Optical lithography was then used to define patterns. To obtain SNW devices with 40 nm pitch fins, 36 nm high and 20 nm wide patterns are first trimmed with Cl_2/O_2 , then transferred into Si-ARC using $\text{CH}_2\text{F}_2/\text{CF}_4/\text{He}$, and lastly followed by HBr/O_2 plasma to etch vertically stacked SiGe/Si multilayers. The etching steps have been performed in an LAM-Versys 2300 ICP tool. Dry (O_2 based plasma in the same etching chamber) and wet cleaning [$\text{SC1}/\text{HF}$ 0.5% + HCl 1% (for 60 s) in a single wafer wet station] steps are necessary to remove the remaining

coatings on the pattern surface. Figure 1 shows the schematic representation of the stack after SNWs etching and subsequent dry- O_2 plus wet cleaning steps.

B. Isotropic etching apparatus and process conditions

Selective etching has been performed in a 300 mm Shibaura CDE-Allegro industrial tool, dedicated to chemical dry etching with an appropriate remote microwave plasma source configuration. The feed gases are excited through the use of a 2.45 GHz microwave applicator coupled with a quartz tube, so the produced plasma species are transported via a teflon tube to the separated reaction chamber. Inside the chamber, the wafer is placed on a chuck-based wafer heating system. In our experiments, the baseline etching process conditions investigated are as follows: gas flows of CF_4 , N_2 , and O_2 are fixed to 200, 200, and 500 SCCM, respectively; microwave power is set to 400 W; pressure in the chamber is regulated to 700 mTorr; and the chuck temperature controlled to be close to 25 °C (\pm 1 °C). The etch time is set to etch 20 nm of Si. To avoid any side effects due to walls material passivation, a seasoning is performed prior to etching experiments by supplying the processing gas in the desired conditions.

C. Characterization of the etched films or structures

1. Blanket film analyses

The etched thickness of Si and SiGe on blanket SOI wafers was measured by spectroscopic ellipsometry (SE) with a J.A.Woollam M2000 tool and an incident angle of 75°. A Cauchy transparent model was used for thickness measurement with wavelengths ranging from 193 to 1700 nm. Roughness modifications, induced by the etching process, were quantified thanks to $1 \times 1 \mu\text{m}^2$ atomic force microscopy (AFM, Bruker Dimension Fastscan) images. The surface composition on Si and SiGe after etching has been evaluated using ToF-SIMS and *ex situ* XPS. TOF-SIMS depth profiling was performed with a 500 eV Cesium ion source for sputtering, with a $300 \times 300 \mu\text{m}^2$ raster and a 25 keV bismuth liquid-metal ion source for analysis and with an $80 \times 80 \mu\text{m}^2$ raster in the center part of the sputter crater.

XPS surface analysis has been performed in a Thermo Fisher Scientific Theta 300 tool equipped with a monochromatic Al $K\alpha$ line x-ray source at 1486.6 eV. For each chemical element detected, time acquisition corresponding to ten scans with a dwell time of 500 ms and a pass energy of 100 eV was used. XPS measurements were taken at 61° from the normal incidence to enhance surface sensitivity. Individual peak contributions in the energy region probed were extracted using a spectral fitting method and then the relative concentration of elements was obtained. Angle resolved XPS was also used quantitatively to measure oxide thickness. The background to this quantification method is described in detail by Thermo-scientific article “Angle resolved XPS.”⁷

2. Pattern analyses

Etched patterns were characterized thanks to 3D and top view scanning electron microscopy (SEM).

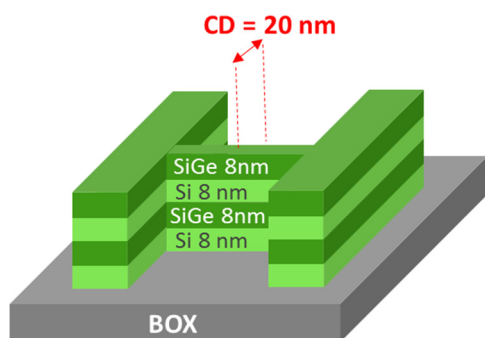


FIG. 1. Schematic of the multilayer stack with its relative individual thicknesses from XRR (x-ray reflectometry).

14 February 2025 09:46:34

III. RESULTS AND DISCUSSION

A. Etch rate variations

1. Influence of O₂ addition

In order to have a better understanding of the role of oxygen addition to an N₂/CF₄ plasma, we have studied the relationship between Si and SiGe etch rates and the oxygen concentration fed in the gas mixture. Figure 2(a) shows Si and SiGe etch rates versus O₂ flow for baseline process conditions as mentioned above (see Sec. II B). Those experiments have been performed on blanket wafers. The SiGe etch rate decreases from 150 nm min⁻¹ (when no O₂ is added in the CF₄/N₂ gas mixture) to almost zero when 500 SCCM of O₂ is added in the gas mixture. For silicon, the etch rate increases

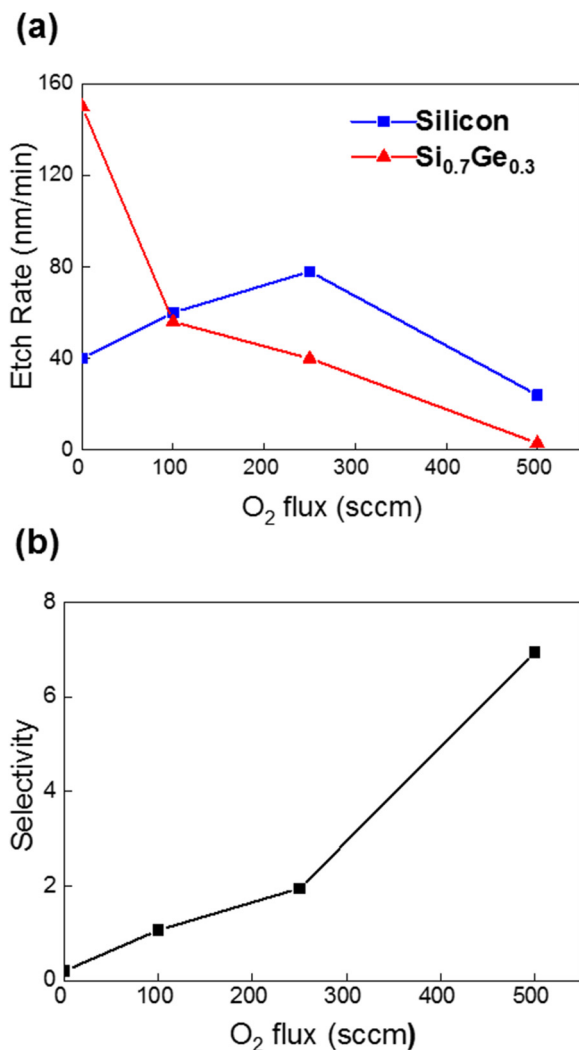


FIG. 2. (a) Si and SiGe etch rates as functions of the O₂ flow variation in the CF₄/N₂ (200/200 SCCM) gas mixture. (b) Selectivity as a function of the O₂ flow.

from 40 nm min⁻¹ (when no O₂ is added) to 78 nm min⁻¹ with 250 SCCM O₂ addition in the gas mixture. For O₂ concentration beyond 250 SCCM, the etch rate drops and reaches 30 nm min⁻¹ at 500 SCCM of injected O₂. Figure 2(b) shows that the Si versus SiGe selectivity dramatically increases with the addition of O₂ and reaches a maximum of 8 at 500 SCCM O₂ added. In the following, the oxygen gas flow will be then set to 500 SCCM in the gas mixture, as it appears as an optimum in terms of selectivity removal between both materials Si and SiGe.

2. Influence of CF₄ addition

In this part, the CF₄ flow has been varied from 0 to 400 SCCM to understand its impact on etching rates and selectivity. CF₄ addition in the gas mixture leads to a linear increase in Si and SiGe etch rates as shown in Fig. 3(a). Si and SiGe etch rates are estimated to be 43 and 10 nm min⁻¹, respectively, when 400 SCCM of CF₄ is added to the gas mixture. Figure 3(b) shows that a maximum selectivity (of 8) is obtained when 200 SCCM of CF₄ is injected in the microwave discharge.

3. Influence of N₂ addition

To quantify the impact of N₂ addition in the gas mixture on Si and SiGe etching rates and selectivity, we have varied the injected N₂ flow from 0 to 400 SCCM. Figure 4(a) shows that the SiGe etch rate drops (from 25 nm min⁻¹ when no N₂ is added to 2 nm min⁻¹ at 400 SCCM N₂ injected) with an increasing amount of N₂. The Si etch rate also decreases for N₂ flows above 50 SCCM (from 40 nm min⁻¹ at 50 SCCM to 10 nm min⁻¹ at 400 SCCM of N₂). As for the selectivity of the process plotted in Fig. 4(b), it is also shown to be greatly influenced by the addition of N₂, with a maximum selectivity obtained for 200 SCCM of injected N₂ in the feed gas mixture.

B. XPS surface analyses

To have a better understanding of the etch rates and selectivity behaviors, XPS analyses have been performed on Si and SiGe.

1. Influence of O₂ addition

Figures 5(a)–5(c) show Si 2p and Ge 3d core level peaks for both amounts of O₂ (low at 100 SCCM and high at 500 SCCM) related, respectively, to the etched Si and SiGe surfaces. The Si 2p spectrum as shown in Figs. 5(a) and 5(b) is deconvoluted into two peaks at 99.4 and 103.5 eV that are attributed to Si–Si bonds and Si–O_x bonds, respectively.⁸ The Ge 3d spectrum in Fig. 5(c) can be divided into two peaks at 29.3 and 32.5 eV coming from Ge–Ge and Ge–O_x bonds, respectively.⁸

For high O₂ percentages, the amount of oxidized Si increases and bulk Si is barely visible, as shown in Fig. 5(a). For the etched SiGe surface and for low amounts of O₂, Si is mostly oxidized compared to Ge. For higher amounts of O₂, only Ge displays a significant increase of oxidized Ge, as seen in Figs. 5(b) and 5(c).

The surface composition given in Figs. 6(a) and 6(b) shows that after etching no nitrogen was detected on the reactive surfaces. Only fluorine, carbon, and oxygen were present on both materials. XPS analyses were performed after an air break. Carbon found on

14 February 2025 09:46:34

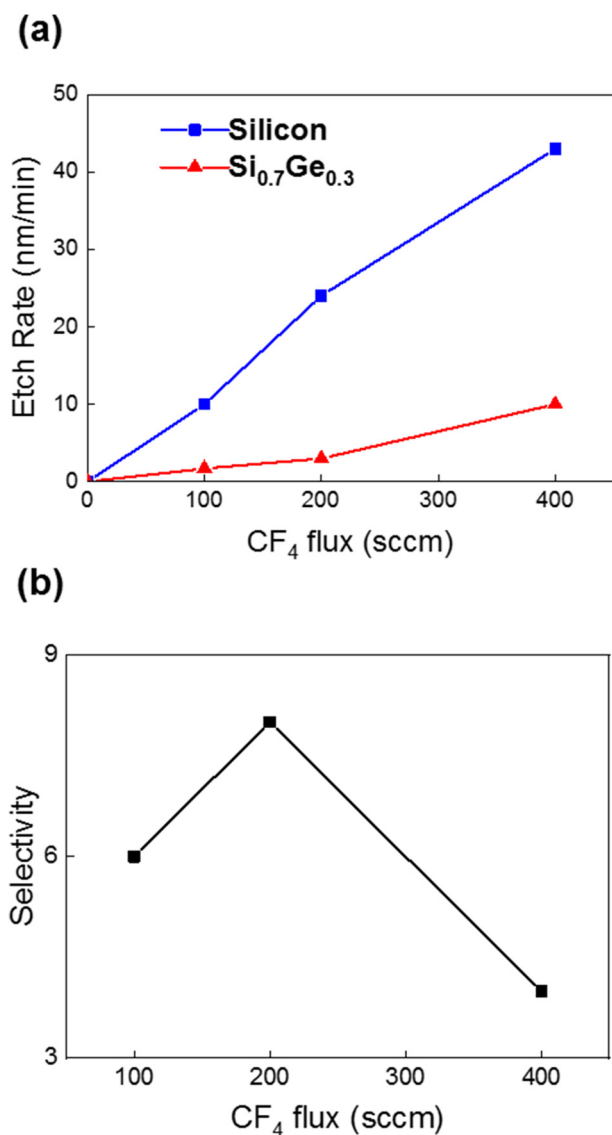


FIG. 3. (a) Si and SiGe etch rates as functions of the CF₄ flow variation in the N₂/O₂ (200 /500 SCCM) gas mixture. (b) Selectivity as a function of the CF₄ flow.

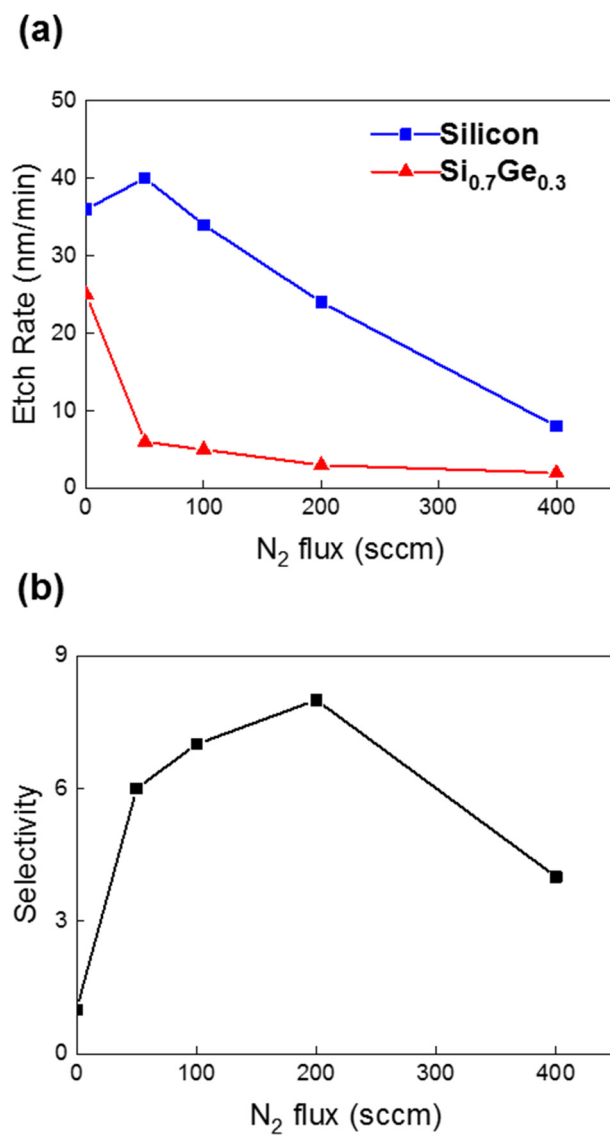


FIG. 4. (a) Si and SiGe etch rates as functions of the N₂ flow variation in the CF₄/O₂ (200 /500 SCCM) gas mixture. (b) Selectivity as a function of the N₂ flow.

the surfaces is, therefore, likely to be due to air contamination while fluorine and nitrogen could have slightly desorbed.

2. Influence of CF₄ addition

Surface compositions have also been investigated for two CF₄ flows (200 and 400 SCCM). Figure 7 shows the surface composition obtained from XPS analysis. It is observed that increasing the amount of CF₄ in the feed gas plasma results in higher fluorine content on top of Si and SiGe etched samples. Indeed, upon addition of 200 and

400 SCCM, the fluorine concentration increases, respectively, from 9% to 18% on Si and from 4% to 8% on SiGe.

3. Influence of N₂ addition

Previous *ex situ* XPS results have all shown that nitrogen is not present on the etched surfaces. Figures 8(a) and 8(b) show the investigated etched Si and SiGe surfaces for two N₂ flows variation set to either 200 or 400 SCCM. Figure 8 shows that an increase of N₂ in the gas mixture leads to a slight increase in the oxygen

14 February 2025 09:46:34

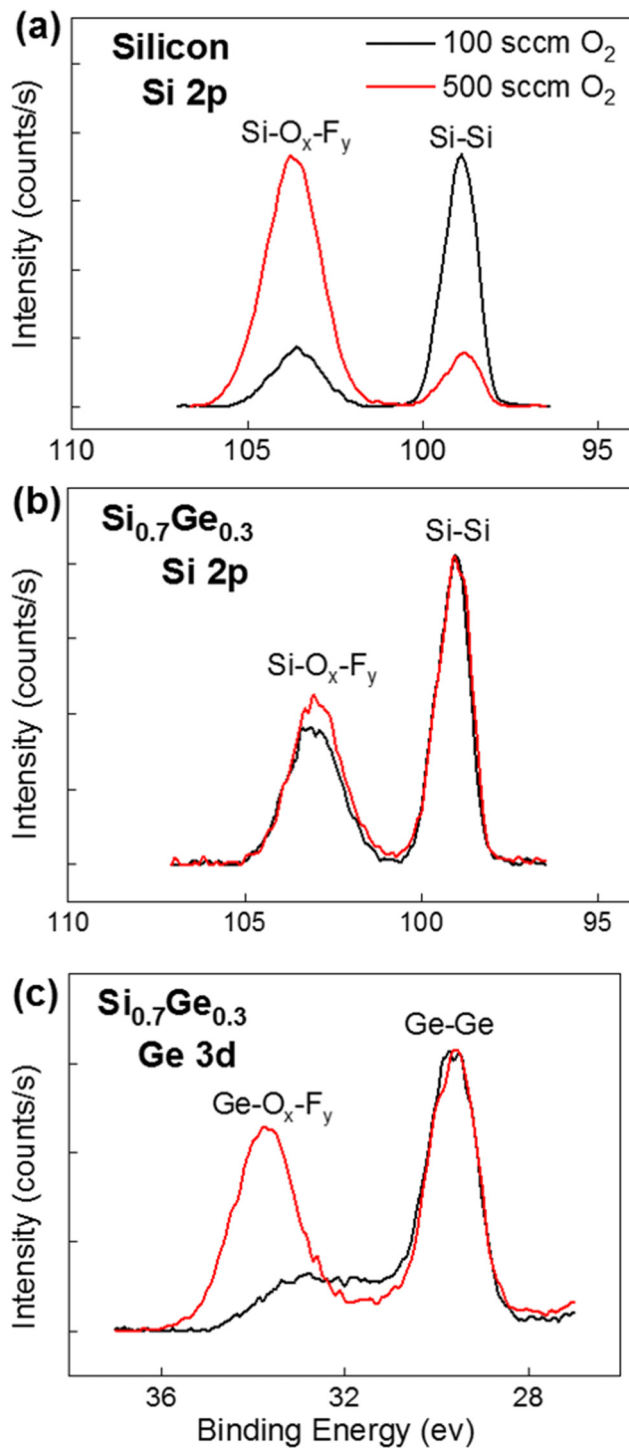


FIG. 5. (a) XPS spectra of Si 2p orbital on the Si sample after etching with O₂ flow of 100 or 500 SCCM. (b) and (c) XPS spectra of Si 2p and Ge 3d orbitals, respectively, on SiGe sample after etching with O₂ flow set to either 100 or 500 SCCM.

amount present on both Si and SiGe etched surfaces. In contrast, we observe a lower amount of adsorbed fluorine on the etched surface of silicon at higher amount of added N₂.

C. Process time impact

In an attempt to gain further insight into Si and SiGe etch rate mechanisms, we have more deeply examined surface modifications after CF₄/N₂/O₂ etchings carried out with the reference process conditions (CF₄/N₂/O₂ = 200/200/500 SCCM, power = 400 W, pressure = 700 W, and T = 25 °C).

We have plotted in Figs. 9 and 10 Si and SiGe etched thicknesses and modified layer thicknesses (measured by ellipsometry) as functions of the etching time.

1. Si sample

Figure 9 shows that the reactive layer thickness increases strongly with the etching time and reaches a maximum of 8 nm after 30 s of etching. Meanwhile, we observe a linear increase in the Si etched thickness with the etching process time.

In order to have a better understanding of this behavior, we have used XPS to evaluate the composition of the reactive layer formed. As shown in Fig. 11, after 30 s of etching, the modified layer reaches not only a stable thickness but also a stable composition. Oxygen, fluorine, and carbon are present on the etched surface. As mentioned previously, carbon is assumed to be due to air exposure. Contributions from the underlying silicon are weak in XPS (Fig. 11), indicating that a thick layer, rich in oxygen and with 10% of fluorine, is indeed formed on a Si substrate after etching. The TEM-energy dispersive x-ray (EDX) image shown in Fig. 12 is also consistent with XPS and spectroscopic ellipsometry results. On this image, we can also notice that the reactive layer is smooth, uniform, and homogeneous in composition. Roughness of this layer was also investigated using AFM characterization. The obtained root mean square (RMS) roughness of the reactive layer on top of the Si etched surface does not exceed 1 nm for all the studied etching times. The etching of silicon through this highly reactive and dynamic SiO_xF_y thick layer can be assisted by NO species that plays an important role in the Si etching mechanism. The presence and the role of NO in CF₄/N₂/O₂ microwave plasma have been discussed in detail by Matsuo *et al.*⁹ It is reported that NO metastable states have an energy of around 6 eV.^{10,11} It can so weaken the oxide bonds with silicon (as in the SiO_xF_y compound) to create free sites for fluorination, resulting in the formation of SiF₄ volatile etchant byproducts. Indeed, these oxide bonds have a binding energy of around 4.7 eV, which is lower than the energy carried by NO species.¹²

2. SiGe sample

Concerning SiGe etch rate variation with etch time, a different behavior from that of silicon is observed (Fig. 10). SiGe is at first slightly consumed when the etching time increases and then reaches a steady state value for slightly more than 100 s etching times. Meanwhile, a 3 nm thick passivation layer is formed promptly (in a few seconds) upon etching and remains constant in thickness afterward. This so-called passivation layer is much thinner than that

14 February 2025 09:46:34

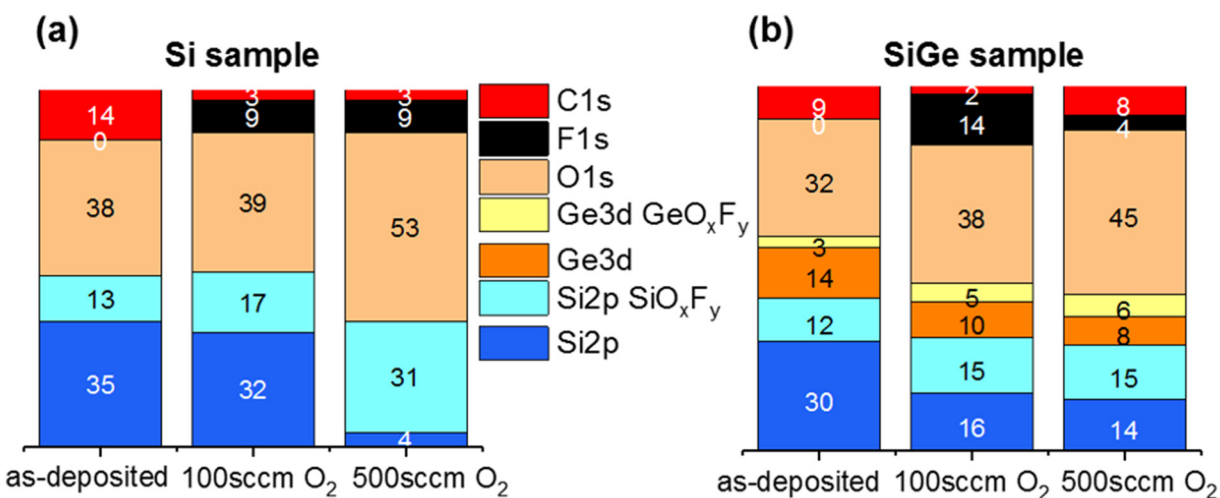


FIG. 6. Comparison of the XPS (at 61°) surface composition of etched Si (a) and SiGe (b) as a function of the O₂ flow set to either 100 or 500 SCCM and as-deposited samples.

formed on silicon. The RMS roughness of the etched samples does not exceed 1 nm.

XPS quantitative measurements displayed in Fig. 13(a) show that the passivation film contains a mixture of oxidized Si, oxidized Ge, fluorine, carbon, and oxygen. Significantly, less fluorine is detected on SiGe surfaces than on Si ones, with relative F atomic concentrations, respectively, estimated to be 4% vs 10% in the depth X-ray probed. The higher amount of carbon on SiGe than on Si surfaces may be due to carbon contamination during the *ex situ* transfer, which is more important relatively on a thinner oxide. From

these data, we have also plotted the evolution of the Ge content in the fraction of the SiGe 30% layer probed by XPS with the etching time as shown in Fig. 13(b). The Ge concentration increases from 30% up to 36%–37% after only 7 s of etching. The TOF-SIMS profile provided in Fig. 14 confirms that an etched SiGe surface is 10% richer in Ge than the as-grown layer. These results suggest that Si is etched preferentially to Ge in the alloy. Thermodynamic data¹³ demonstrate that Si etching by SiF₄ formation is indeed favored compared to Ge etching by GeF₄ formation, resulting in higher Ge content etched surfaces,

14 February 2025 09:46:34

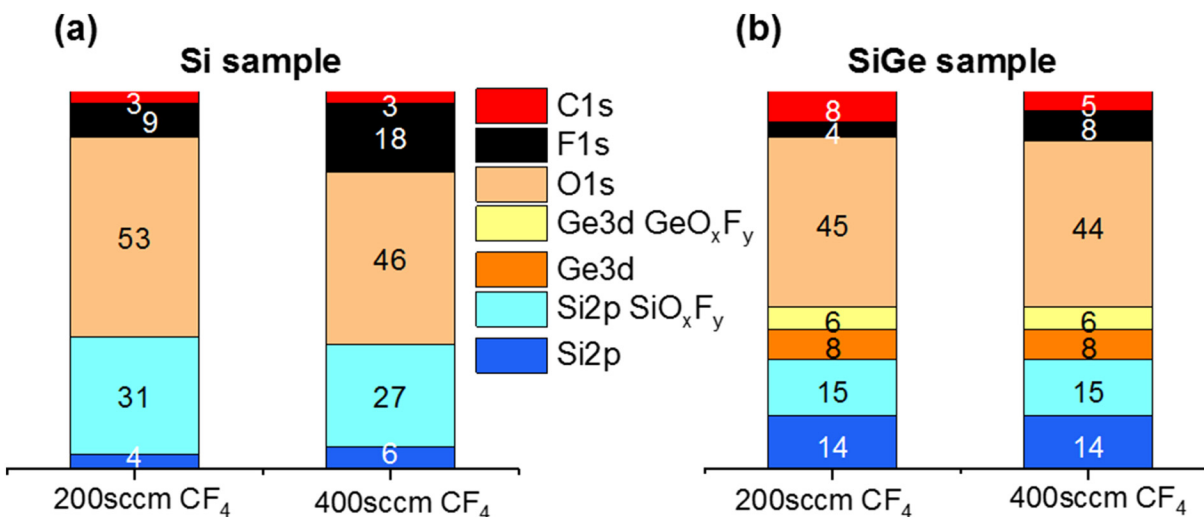


FIG. 7. XPS surface composition (at 61°) of the etched Si (a) and SiGe (b) for two CF₄ flows set either to 200 or 400 SCCM.

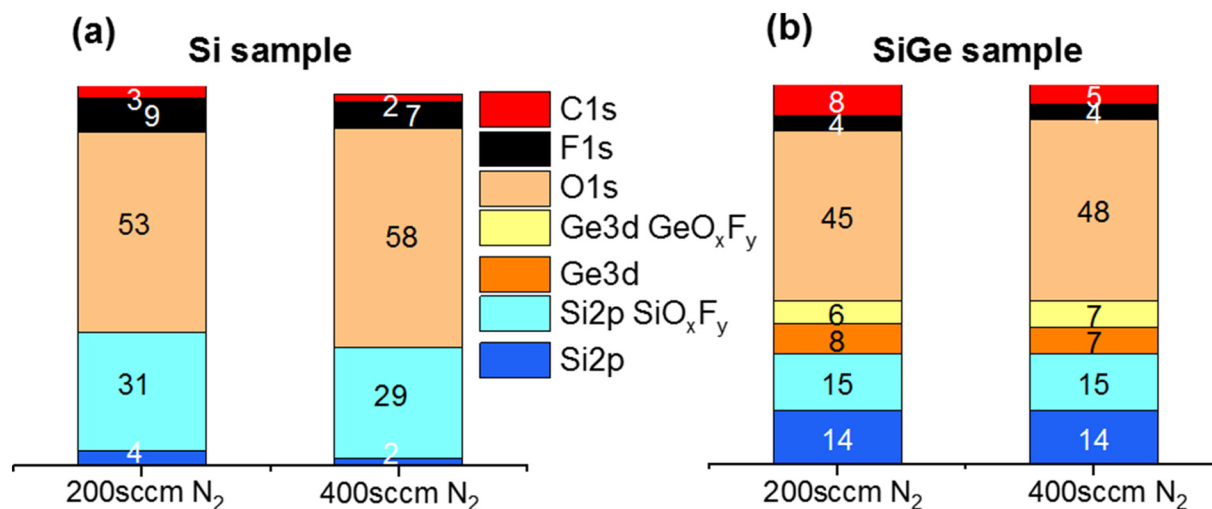


FIG. 8. XPS surface composition (at 61°) of the etched Si (a) and SiGe (b) for two N₂ flows set either to 200 or 400 SCCM.

- (1) $\text{Si}_{(s)} + 4\text{F}_{(g)} \rightarrow \text{SiF}_{4(g)} \Delta_f H^\circ(\text{SiF}_4) = -1614.9 \text{ kJ mol}^{-1}$
- (2) $\text{Ge}_{(s)} + 4\text{F}_{(g)} \rightarrow \text{GeF}_{4(g)} \Delta_f H^\circ(\text{GeF}_4) = -1190 \text{ kJ mol}^{-1}$
- (3) $T_{\text{boiling}}^{\text{GeF}_4} = -36.5^\circ\text{C} > T_{\text{boiling}}^{\text{SiF}_4} = -86^\circ\text{C}$

D. Discussion and proposed etch mechanism

We have previously observed a significant etch rate drop for both Si and SiGe when increasing O₂ amount beyond 250 SCCM in the feed gas plasma leading to higher selective etch of Si to SiGe. Based on XPS data (Figs. 5 and 6), this trend can be explained by surface oxidation. These results suggest that, unlike Si, spontaneous oxidation of SiGe in the presence of oxygen is straightforwardly correlated to the linear etch rate decrease as previously shown.¹⁴⁻¹⁶

Indeed, Si-Ge bonds (with a binding energy of 296 kJ mol⁻¹) are weaker and so easier to break compared to Si-Si bonds (with a binding energy of 325 kJ mol⁻¹). Concerning the observed etch rate increase of Si at the low stage of added O₂ (below 250 SCCM of O₂), the mechanism behind this etch rate trend remains unclear. One may, however, suspect that the addition of a small amount of O₂ increases the F atomic concentration through an oxidation of CF_x radicals as also reported by Oehrlein *et al.*¹⁷ By the same logic and in agreement with several published papers,^{18,19} the kinetics and XPS results we have viewed when injecting CF₄ in the feed gas plasma result in a rich F atomic gas phase that leads to higher adsorbed fluorine on the etched surfaces and so to higher etching rates for both studied materials. The observations concerning etch

14 February 2025 09:46:34

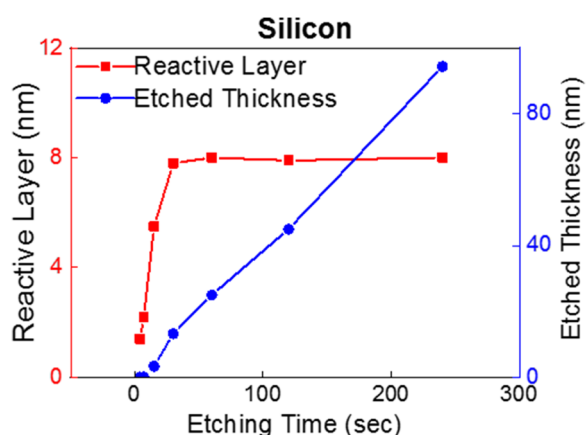


FIG. 9. Si etched thickness and reactive layer thickness as a function of the etching time.

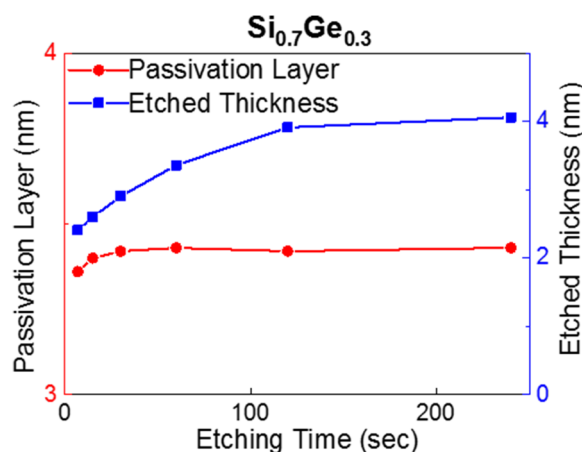


FIG. 10. Etched thickness and passivation layer thickness on SiGe as functions of the etching time (using the baseline etching process).

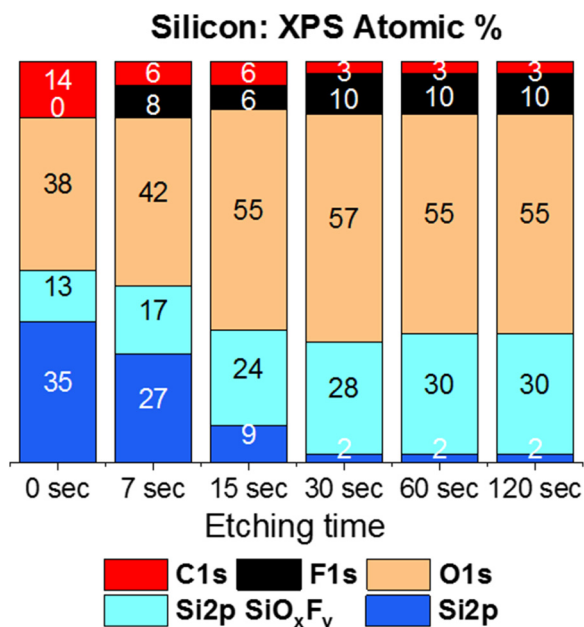


FIG. 11. XPS surface composition (at 61°) of Si surface as a function of the etching time using the baseline process.

rates decrease and etched surfaces' composition when adding N₂ in the injected feed gas are likely due to N₂ species that have an impact on the dissociation of injected O₂ and CF₄ species like that explained by Matsuo *et al.*⁹ The gas phase is richer in oxygen atoms (when increasing N₂ added amount) that are adsorbed on the surface, resulting in an etch rate decrease.

Based on these trends and the results obtained in Sec. III B, Si and SiGe etching mechanism is so proposed, which sheds some light on the selective etching of Si compared to SiGe with CF₄/N₂/O₂ based plasmas. In agreement with Caubet *et al.*,¹⁸ Si and SiGe etchings simultaneously occur with surface passivation by oxygen

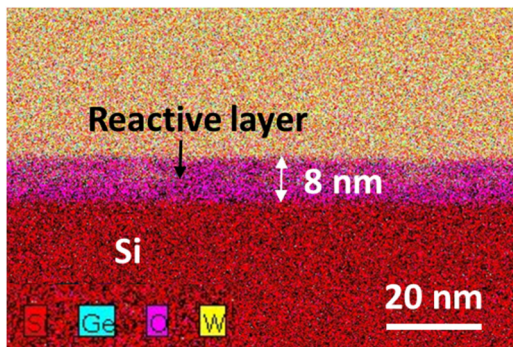


FIG. 12. Cross-sectional TEM-EDX image of a Si substrate after 30 s of etching using the baseline process (200 SCCM CF₄/200 SCCM N₂/500 SCCM O₂), with the presence of a 2D SiO_xF_y reactive layer.

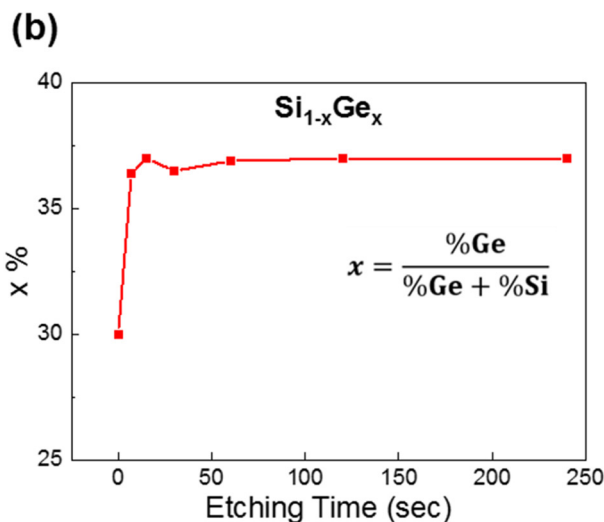
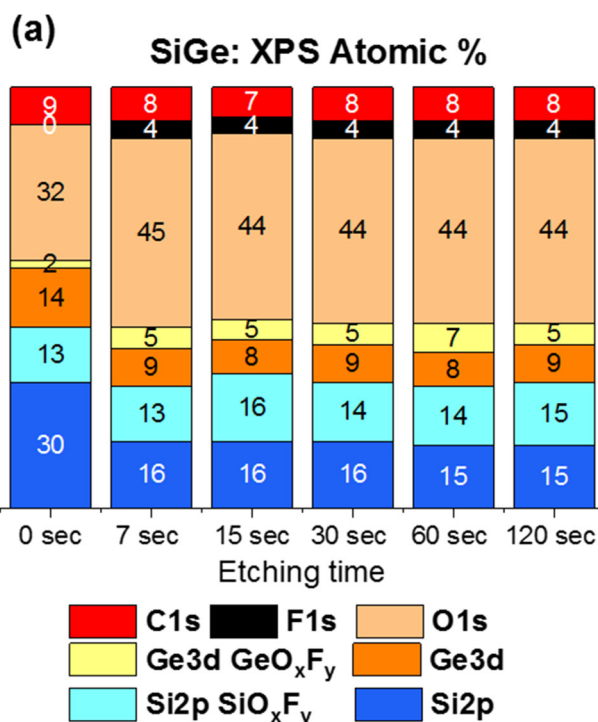


FIG. 13. (a) XPS chemical composition (at 61°) of a SiGe surface as a function of the etching time (using the baseline etching process). (b) Ge fraction in the alloy probed by XPS as a function of the etching time [the Ge content in the bulk of the SiGe layer (prior to etching) was 30%].

and etching by fluorine assisted by NO species (as explained in Sec. III B). An oxygen rich gas phase results in a rapid formation of a smooth, thin, and self-limited passivation layer on a SiGe surface, which contains SiO_xF_y and GeO_xF_y mixtures. When SiGe is exposed to etchants, fluorine preferentially etches Si atoms in the

14 February 2025 09:46:34

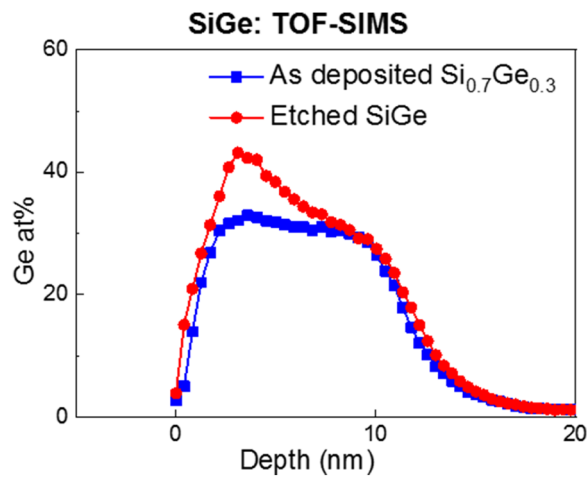


FIG. 14. TOF-SIMS Ge concentration depth profile in as-grown and etched SiGe (using the baseline etching process).

alloy as explained above. There is then less fluorine for Ge to react with, resulting in a lower etch rate of Ge compared to that of Si. The latter phenomenon results in a Ge enrichment of the SiGe surface. The Ge active sites, created under the impact of NO radicals that weaken Ge–O bonds (with bond strength inferior to 6 eV in GeO_xF_y compound²⁰), are progressively occupied by oxygen since the covering rate of the surface by fluorine atoms becomes smaller. The SiGe etch rate decelerates and becomes definitely lower than that of pure Si. Though no real-time surface analysis experiments were conducted, *ex situ* composition measurements of Si and SiGe surfaces after etching proved to be useful for further insight. In apposition to SiGe, a quite thick and remarkably reactive SiO_xF_y layer is formed on pure Si with our etching process conditions. This layer is highly dependent on the injected feed gas ratio. Within several seconds of etching, this layer reaches its saturation thickness while remaining smooth. It then stops evolving.

E. Optimization of the etch process selectivity on blanket wafers: Influence of pretreatments on selectivity

Data above have shown that the CDE (chemical dry etching) process is driven by complex surface etching reactions. Surface oxidation during etching definitely impacts etch rates and leads to selectivity changes.

A study of the impact of different types of pretreatments on surface composition and therefore etch rates is thus of tremendous interest, as it is oxidation differences between Si and SiGe that could yield the best selectivity. Parameters for dry and wet oxidation were selected here in order to form thin oxides.

Si and SiGe layers were deoxidized prior to oxidation and etching experiments. The etch time is set to etch 20 nm of Si. Our based process ($\text{CF}_4/\text{N}_2/\text{O}_2 = 200/200/500$ SCCM, power = 400 W, pressure = 700 W, and $T = 25^\circ\text{C}$) was used for etching. Table I shows the evolution of etch selectivity (of Si over SiGe 30%) with different oxidation pretreatments. All the pretreatments improve

TABLE I. Si over SiGe 30% etch selectivity as a function of the oxidizing treatment used beforehand.

Pretreatments	Si:SiGe selectivity
Deoxidation (HF 1%)	4
Dry oxidation (at 350 °C)	10
Wet H_2O_2 (in H_2O) treatment	7
Wet hot standard cleaning 1 treatment ($\text{NH}_4\text{OH}/\text{H}_2\text{O}_2/\text{H}_2\text{O}$)	7
Wet O_3 (in H_2O) treatment	6
Without pretreatment	8

selectivity compared to deoxidation (only). Dry oxidation using an O_2/N_2 (76%/14%) based plasma gives the highest selectivity, i.e., 10. Note that the addition of this small amount of nitrogen to O_2 based plasma allows a higher dissociation degree of O_2 molecules resulting in an atomic-oxygen rich gas phase.²¹

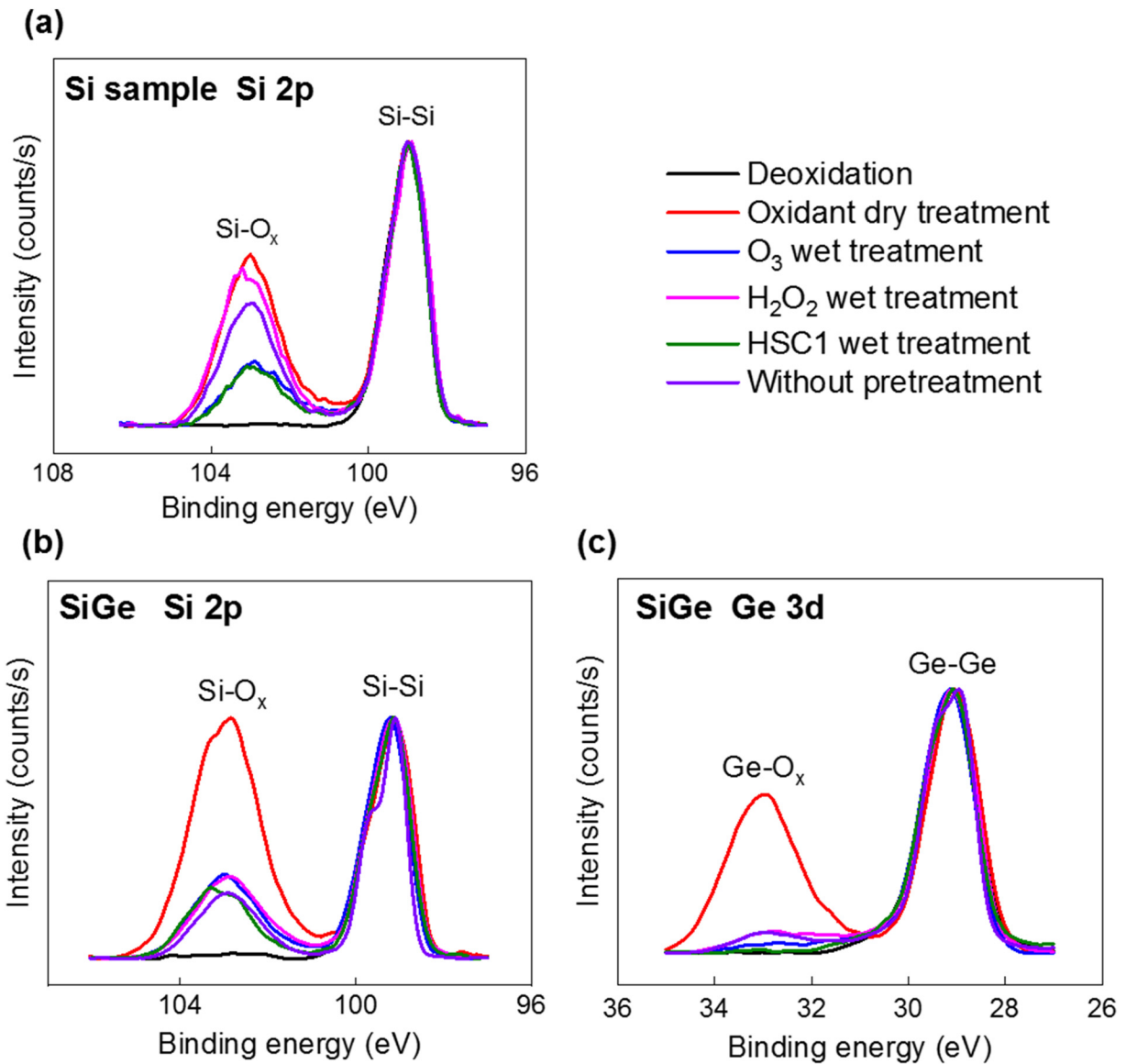
XPS analyses give access to the surface oxidation state and allow to estimate the overlayer thickness after various types of oxidation performed on Si and SiGe.⁷ We focus on the evolution of the Si 2p peak for each type of oxidation for silicon, as shown in Fig. 15(a). Si–Si bonds are transformed into Si–O bonds when a Si surface is exposed to oxidizing chemicals. A double peak structure with a 4 eV separation is observed; those peaks are due to Si and SiO_2 , respectively. All curves were normalized to the intensity of Si^{0+} (Si–Si peak) signals. The SiO_2 peak is the highest component after dry oxidation, with a layer thickness of 1.2 nm (see Table II), while for other pretreatments, the oxidation thickness is 1.1, 0.5, and 0.6 nm after Wet H_2O_2 treatment, Wet hot SC1 treatment, and Wet O_3 (in H_2O) treatment, respectively.

Both Si 2p and Ge 3d peaks were investigated for SiGe, as shown in Figs. 15(b) and 15(c). Same as Si 2p peaks, all Ge 3d curves were normalized to the intensity of Ge^{0+} signals. The presence of Si–O (103.5 eV) and Ge–O (32.5 eV) bonds resulting from the interaction between silicon and germanium atoms and oxygen are also the highest contributions through the dry oxidation treatment. The oxide thickness is thicker on SiGe than on Si (2 nm instead of 1.2 nm). This is likely due to an oxidation rate that is higher on SiGe compared to bulk Si during the initial oxidation stage. This may be attributed to the weaker Si–Ge binding energy than the Si–Si one (296 vs 325 kJ mol^{-1} , respectively). By contrast, the oxide is typically less than 1 nm thick and approximately the same for SiGe and bulk Si after wet oxidation using H_2O_2 (in H_2O), HOT SC1, or O_3 (in H_2O) based wet chemistry. This is likely due to the solubility of GeO_2 in H_2O based wet chemistries, as confirmed by XPS spectra. The intensity of the oxidized Ge peak is very low compared to that of silicon oxide. These data are in line with selectivity results. Indeed, dry oxidation leads to thicker passivation layers on SiGe than on Si for the same conditions. The SiGe etch rate is then decreased compared to the Si etch rate, resulting in a higher selectivity.

F. Application on patterned wafers

In this part, we have evaluated the etching of patterned structures composed twice of 8 nm thick Si and 8 nm thick SiGe 30% layers (as shown in Fig. 1). In this part, only the critical dimension

14 February 2025 09:46:34



14 February 2025 09:46:34

FIG. 15. (a) XPS spectra, performed at 61° , of Si 2p orbitals on bulk Si surfaces after different types of oxidation. XPS spectra of Si 2p (b) and Ge 3d (c) orbitals on SiGe 30% sample after different types of oxidation.

(CD) of devices of interest will be presented before and after the etching process. Figure 16 shows a top view image of the as-deposited stack after patterning.

In a first set of experiments, patterned wafers have been deoxidized in diluted HF and etched with our based etching process ($\text{CF}_4/\text{N}_2/\text{O}_2 = 200/200/500$ SCCM, power 400 W, $P = 700$ mT, and $T = 25^\circ\text{C}$) with an etching time such that 20 nm wide SiGe 30% nanochannels would be fully released.

As seen in Fig. 17, SiGe CD is thinned during the etching of Si, meaning that it is also consumed during etching. The SEM image

TABLE II. Si and SiGe oxide thicknesses from XPS after various types of oxidations.

Pretreatments	Oxide thickness (\AA)	
	Si	SiGe
Deoxidation	0.4	1
Dry oxidant treatment	12	20
Wet H_2O_2 treatment	11	9
Wet hot SC1 treatment	5	7
Wet O_3 (in H_2O) treatment	6	8

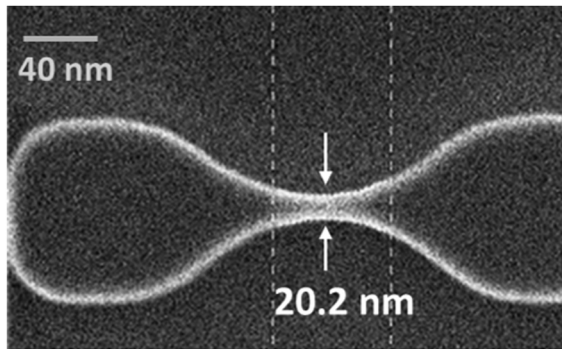


FIG. 16. Top view image of 20 nm wide pattern made of Si/SiGe 30 %/Si/SiGe30 % on top of a buried oxide (SOI starting substrate).

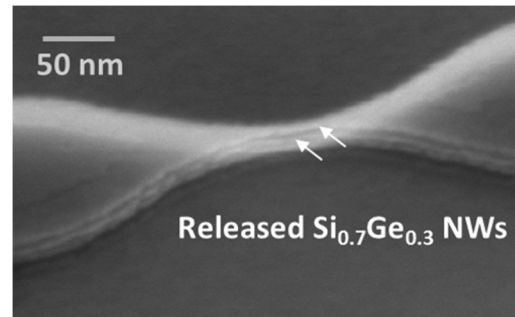


FIG. 19. 3D SEM image of two released SiGe nanowires of 20 nm wide and 8 nm thick (at constriction) after the use of dry oxidation prior to selective etching (using the baseline etching process). Wider regions on each side of the constrictions are sources and drains actually.

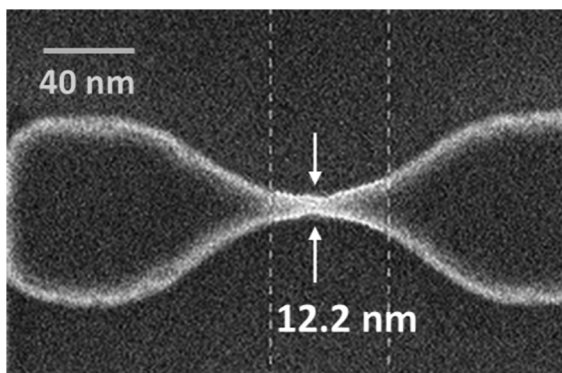


FIG. 17. Top view SEM image of a patterned device after etching (using the baseline etching process).

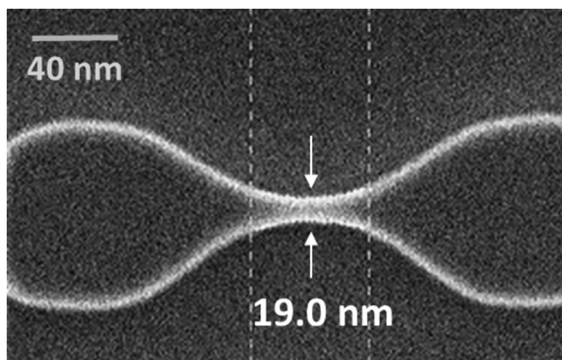


FIG. 18. Top view SEM image of a pattern after the use of dry oxidation prior to selective etching (using the baseline etching process). SiGe width is almost intact.

clearly shows that SiGe CD is thinned down to almost half its original width (~12 nm wide compare to 20 nm observed in Fig. 16).

The benefit of dry oxidation pretreatment addition previously shown on the blanket wafer is now evaluated on patterned wafers. Figure 18 shows that with dry oxidation pretreatment addition, SiGe nanowires have a width definitely closer to the as-grown values (~19 nm wide) with dry oxidation prior to etching. Selectivity seems to be improved (superior to 10) and sufficient to obtain totally released 20 nm wide and 8 nm thick SiGe stacked nanochannels, as shown in the SEM image in Fig. 19.

IV. CONCLUSION

We have studied the dry etching of blanket Si and SiGe layers with different surface characterization techniques. XPS results were consistent with etch rate evolutions: the addition of oxygen to the CF_4/N_2 feed gas in microwave discharge resulted in a decrease of Si and SiGe 30% etching rates through the formation of oxygen rich ad-layers on the etched surfaces. When the gas phase was sufficiently rich in oxygen, the etching selectivity of Si versus SiGe increased. A detailed analysis of XPS spectra showed that an 8 nm thick reactive layer made of SiO_xF_y was formed on Si during etching. Meanwhile, a thin (~3 nm only) passivation layer made of SiO_xF_y and GeO_xF_y was formed on SiGe during etching, which protected the alloy. TOF-SIMS depth profiling evidenced a 10% Ge enrichment on the surface after etching. We otherwise showed that oxidizing treatments carried out prior to etching resulted in the formation of thin oxide ad-layers on Si and SiGe and increased process selectivity. Siliconlike oxides were formed upon wet oxidation on SiGe surfaces, which were slightly thicker than oxides formed on silicon. The highest selectivity was obtained after dry oxidation. This is likely due to the formation of a mixture of GeO_x and SiO_x , with an oxide on SiGe 30% that is definitely thicker than on Si.

Patterned wafers were also investigated. The same etching conditions than those preoptimized on fullsheet wafers were used to laterally etch Si in stacks made of 8 nm thick Si and SiGe 30% layers and 20 nm wide. SiGe nanowires were consumed and thinned down to half the original value when starting from deoxidized surfaces. In

14 February 2025 09:46:34

order to improve etching selectivity on patterns, dry oxidation was performed prior to etching. Only a slight consumption of SiGe nanowires (0.5 nm from each side of the SiGe device) was then evidenced by the Top-View SEM CD investigation, which clearly showed that the etching selectivity was drastically improved.

ACKNOWLEDGMENT

This work was supported by the French National Research Agency (ANR) within the IMPACT program under Contract No. ANR-10-EQPX-33.

REFERENCES

- ¹X. Deyuan, W. Xi, Y. Haijiang, Y. Yuehui, X. Zhifeng, and C. Minhwa, *J. Semicond.* **30**, 014001 (2009).
- ²D. Sacchetto, M. H. Ben-Jamaa, G. DeMicheli, and Y. Usuf Leblebici, *Proceedings of the European Solid State Device Research Conference, 2009. ESSDERC '09*, 14 September 2009 (IEEE, Athens, 2009), pp. 245–248.
- ³S. Barnola *et al.*, *ECS Trans.* **16**, 923–934 (2008).
- ⁴G. K. Chang, T. K. Carns, S. S. Rhee, and K. L. Wang, *J. Electrochem. Soc.* **138**, 202 (1991).
- ⁵F. Schäffler, *Semicond. Sci. Technol.* **12**, 1515 (1997).
- ⁶R. Loo *et al.*, *ECS J. Solid State Sci. Technol.* **6**, P14 (2017).
- ⁷Thermo Scientific, *Angle Resolved XPS* (2008).
- ⁸J. F. Moulder and J. Chastain, *Handbook of X-Ray Photoelectron Spectroscopy: A Reference Book of Standard Spectra for Identification and Interpretation of XPS Data* (Perkin-Elmer Corporation, Eden Prairie, MN, 1992).
- ⁹P. J. Matsuo, B. E. E. Kastenmeier, G. S. Oehrlein, and J. G. Langan, *J. Vac. Sci. Technol. A* **17**, 2431 (1999).
- ¹⁰M. G. Blain, T. L. Meisenheimer, and J. E. Stevens, *J. Vac. Sci. Technol. A* **14**, 2151 (1996).
- ¹¹J. Amouroux, S. Cavvadias, and D. Rapakoulias, *Rev. Phys. Appl.* **14**, 969 (1979).
- ¹²V. Raballand, *Gravure en plasma dense fluorocarboné de matériaux organosiliciés à faible constante diélectrique (SiOCH, SiOCH poreux). Etude d'un procédé de polarisation pulsée* (Université de Nantes, Nantes, 2006).
- ¹³T. Allison, *NIST-JANAF Thermochemical Tables* (NIST, Gaithersburg, 1998).
- ¹⁴S. Margalit, A. Bar-Lev, A. B. Kuper, H. Aharoni, and A. Neugroschel, *J. Cryst. Growth* **17**, 288 (1972).
- ¹⁵H. K. Liou, P. Mei, U. Gennser, and E. S. Yang, *Appl. Phys. Lett.* **59**, 1200 (1991).
- ¹⁶F. Rozé, O. Gourhant, E. Blanquet, F. Bertin, M. Juhel, F. Abbate, C. Pribat, and R. Duru, *J. Appl. Phys.* **121**, 245308 (2017).
- ¹⁷G. S. Oehrlein, P. J. Matsuo, M. F. Doemling, N. R. Rueger, B. E. E. Kastenmeier, M. Schaepkens, T. Standaert, and J. J. Beulens, *Plasma Sources Sci. Technol.* **5**, 193 (1996).
- ¹⁸V. Caubet, C. Beylier, S. Borel, and O. Renault, *J. Vac. Sci. Technol. B* **24**, 2748 (2006).
- ¹⁹G. S. Oehrlein and H. L. Williams, *J. Appl. Phys.* **62**, 662 (1987).
- ²⁰J. R. Rumble, *CRC Handbook of Chemistry and Physics*, 98th ed. (CRC, Boca Raton, FL, 2017).
- ²¹Y. Ichikawa, T. Sakamoto, A. Nezu, H. Matsuura, and H. Akatsuka, *Jpn. J. Appl. Phys.* **49**, 106101 (2010).